Wave Inversion Technology, Report No. 4, pages 63-75

Seismic migration by demodeling

J. Schleicher, L.T. Santos, and M. Tygel[1]

keywords: *seismic migration, inverse Kirchhoff, demodeling*

ABSTRACT

We numerically investigate the inverse operation to the classical Kirchhoff-Helmholtz integral. This operation, which we call Kirchhoff demodeling, is completely analogous to the forward modeling operation. In the same way as the latter integrates along the depth reflector, the new inverse demodeling operation integrates along the corresponding reflection traveltime surface. The result is a seismic pulse at the reflector depth, multiplied with the corresponding reflection coefficient. In this way, we have a new and promising migration technique at hand. We will refer to this method as migration by demodeling, in accordance to its position in the triangle of modeling, migration, and modeling by demigration. A particular attraction of the proposed migration method is that it is a much faster process than conventional Kirchhoff migration, even when applied with full true-amplitude weights. Demodeling is a target-oriented operation as it can be restricted to a target reflector. Demodeling requires an identification and picking of the events to be migrated. This should, however, not pose a severe restriction to the applicability of the method since the identification of horizons of interest is always necessary at some stage of the seismic processing sequence. In this sense, the new process is not be seen as replacement of Kirchhoff migration, but as an alternative and complementary procedure. Possible applications include the fast true-amplitude migration of an identified event to determine whether a promising AVO trend in the CMP section is confirmed after migration.

INTRODUCTION

Wave propagation in acoustic media can be described by the Kirchhoff integral (Sommerfeld, 1964). So, a natural idea is to use this integral to solve the inverse problem, that is, to reconstruct the medium of propagation form the recorded wavefield. As is well-know, however, the Kirchhoff integral cannot be used for backward propagation because it yields zero if the receiver is within the closed surface over which is integrated (Langenberg, 1986). A correct inversion is also impossible because then the

[1]**email:** js@ime.unicamp.br,lucio@ime.unicamp.br

evanescent parts of the wave field explode. To overcome this problem, one usually works with the complex conjugate of the Kirchhoff integral (Porter, 1970; Bojarski, 1982). In this way, the nonevanescent parts of the wave field are correctly backpropagated whereas the evanescent parts are exponentially damped. This approach leads to the well-known Kirchhoff migration as is used today in practice (Schneider, 1978). The same migration operator results from a geometrical approach which implies summing up all possible contributions of a single 'diffraction point' in the wave field. It turns out that migration can be realized by a weighted stack along the diffraction-traveltime (or Huygens) surfaces (Rockwell, 1971).

Most recently, however, a different approach was used to set up an approximate inverse operation to the Kirchhoff forward-modeling integral in Kirchhoff-Helmholtz approximation (Tygel et al., 2000). The new inverse Kirchhoff-Helmholtz integral is formed in a completely analogous way to the original forward integral by substituting all kinematic quantities by their corresponding dual ones in accordance with the duality relationships derived by (Tygel et al., 1995). For example, the integration along the reflector is substituted by one along the reflection-traveltime surfaces. The weight factor is then obtained by the criterium that the output amplitude of the inverse integral should be identical to the input amplitude of the forward integral.

The new inverse integral can be used in seismic imaging to design a new migration technique. Because of its asymptotic inverse relationship to forward modeling by the Kirchhoff integral, we refer to the new migration technique as Kirchhoff demodeling. In this paper, we present synthetic examples on simple earth models of how the demodeling integral can be employed for the purpose of a seismic true-amplitude migration.

Note that the new Kirchhoff-Helmholtz migration is even more economic than conventional Kirchhoff migration. Instead of all possible diffraction-traveltime surfaces, only the true reflection-traveltime surfaces are needed as stacking surfaces. This makes Kirchhoff demodeling also a target-oriented process. However, where conventional Kirchhoff migration can be restricted to a *target zone* (that may ore may not contain one or many reflectors) Kirchhoff demodeling can be restricted to a *target reflector*. Of course, there is a price to be payed. The drawback of Kirchhoff demodeling is that the reflection-traveltime surfaces have to be indentified and picked before they can be migrated. On the other hand, the identifying and picking has generally to be done anyway at some stage of the seismic processing sequence.

Once the reflection-traveltime surfaces are picked and the trace amplitudes along them are known, it is sufficient to perform the very same stack along them for any arbitrary depth point. The only quantity that changes in the process as a function of the depth point to be migrated is the weight function. The result of this procedure is a true-amplitude migrated image equivalent to what is obtained after a conventional true-amplitude Kirchhoff migration.

The details of the theory involved in setting up the mentioned inverse Kirchhoff-Helmholtz integral can be found in (Tygel et al., 2000). A derivation of the constant-velocity formulas that were used in the present implementation is given in the Appendix. The main purpose of this paper is to address the more practical aspects of Kirchhoff demodeling. For this aim, we study the procedure numerically and compare its results to those of conventional Kirchhoff migration.

NUMERICAL ANALYSIS

To verify the validity of the demodeling integral, we have designed a couple of simple numerical experiments.

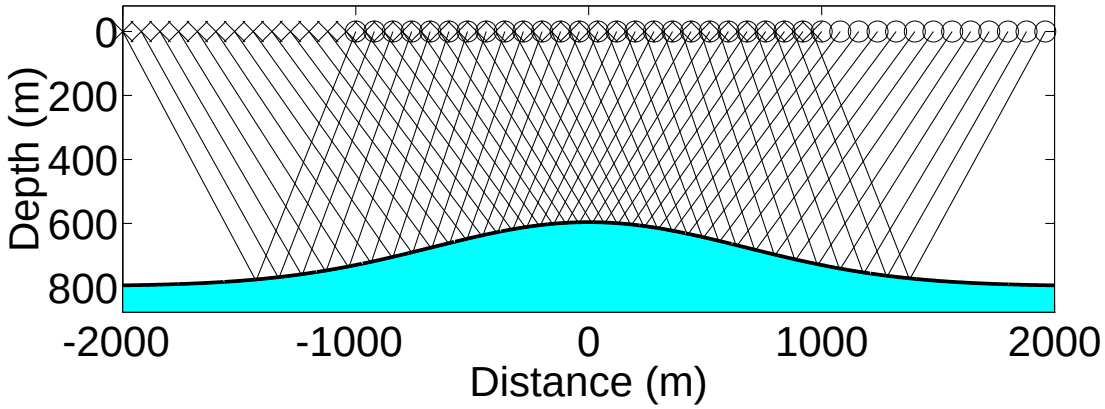

Figure 1: Model I: A slightly curved interface below a homogeneous overburden.

The first one is a seismic common-offset experiment with a half-offset of h =500 m, simulated above the earth model depicted in Figure 1. It consists of two homogeneous acoustic layers with constant velocities of 4 km/s and 4.5 km/s, respectively, separated by a smooth interface in the form of a dome structure. The top of the dome is at 600 m depth, and its base is at 800 m. The terminology 'common-offset experiment' means that all source-receiver pairs involved are separated by the same fixed source-receiver distance (offset) of $2h = 1000$ m. The common-offset section was generated by a ray tracing algorithm using a symmetric Ricker wavelet (Ricker, 1953) of unit peak amplitude and of duration of $T = 64$ ms, i.e., with a dominant (peak) frequency of about 30 Hz. In order to perform the demodeling integral, it is necessary to extract the traveltime curve and the amplitudes of the seismic reflection event. This was done by an automatic picking process.

In Figure 2, we compare the demodeling result with the corresponding Kirchhoff depth migrated section (every fifth trace is shown). Like Kirchhoff migration, also demodeling provides an image with wavelets perfectly aligned along the reflector, which

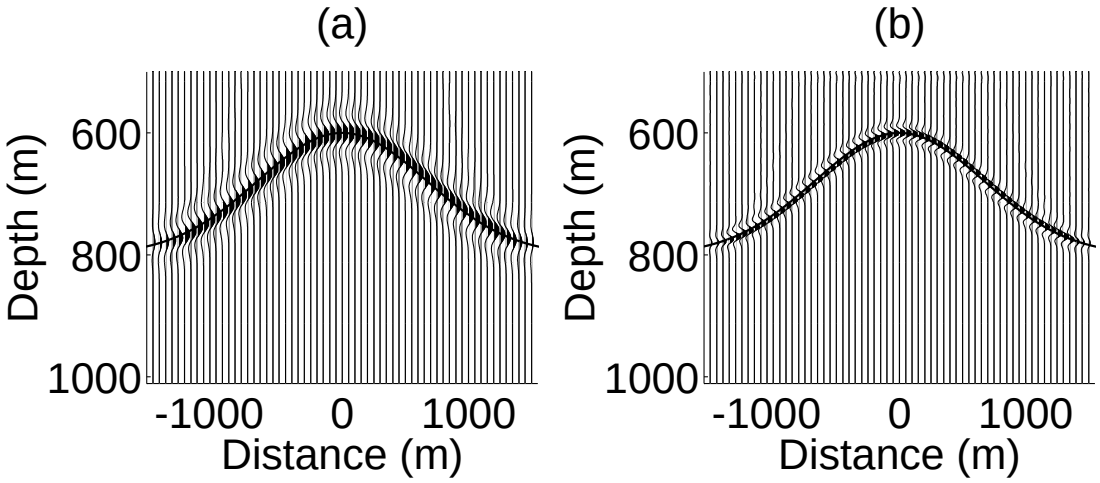

Figure 2: (a) Kirchhoff depth migrated section, (b) Kirchhoff demodeled section, of noise-free common-offset data for Model I.

is indicated by a continuous line. This confirms that demodeling correctly positions the reflector in depth.

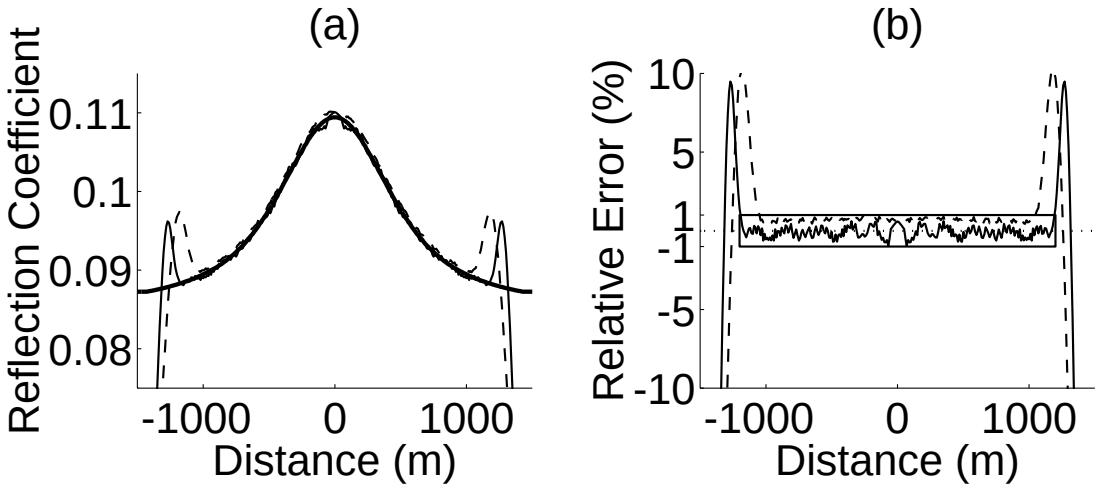

Figure 3: (a) Amplitudes along the reflector from demodeling (solid line) and Kirchhoff migration (dashed line) in comparison to reflection coefficients (bold line). (b) Relative errors.

To check on the amplitudes, Figure 3a compares the obtained peak amplitudes along the reflector from demodeling and Kirchhoff migration with the theoretical values of the reflection coefficient.

We observe an almost perfect coincidence between the migrated amplitudes (thin and dashed lines) and the theoretical curve (bold line) in a large region in the center

of the figure. On both sides, a larger error can be observed that is due to boundary effects. In the boundary region, data are missing, which leads to an uncomplete reconstruction of the true amplitudes. Note that the boundary zone of demodeling is visibly smaller than that of Kirchhoff migration. Figure 3b quantifies the relative amplitude errors of both migration methods. In the central region, the errors fluctuate around a mean value of about one half of one percent, never exceeding one percent, as indicated by the box. This error of about 1% is due to numerical effects and can be further reduced by reducing the temporal and spatial sampling rates. These results confirm that the demodeling integral constitutes an asymptotic inverse to the well-known forward Kirchhoff-Helmholtz integral. Moreover, we see that under ideal circumstances the image quality achieved by demodeling can be superior to that of Kirchhoff migration.

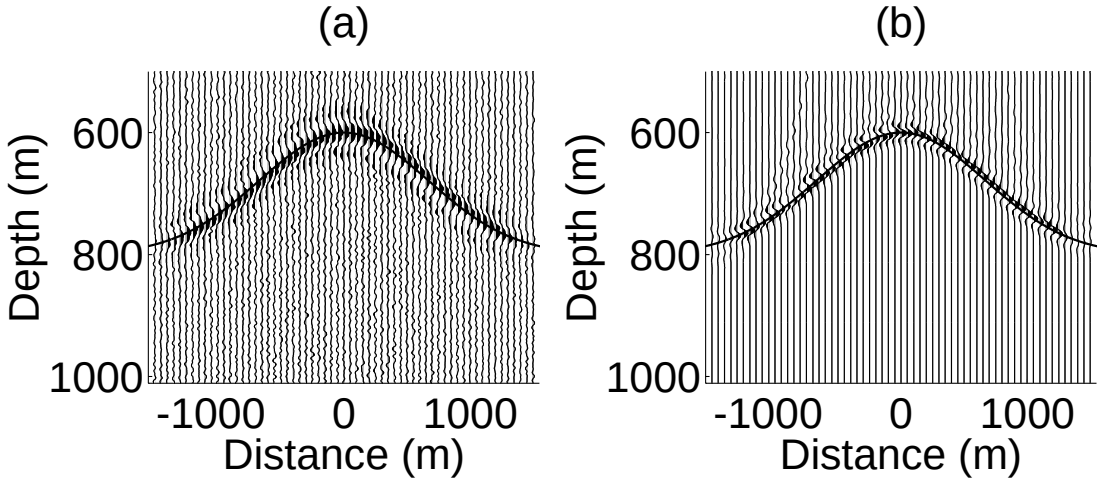

Figure 4: (a) Kirchhoff depth migrated section, (b) Kirchhoff demodeled section, of noisy common-offset data for Model I.

To test demodeling under more realistic conditions, we have repeated the above experiments adding white noise with signal-to-noise ratio 3 to the ray data. The resulting migrated sections are depicted in Figure 4. As expected, the kinematics is not affected by the noise. As an advantage of demodeling, we observe that off the reflector the noise level is much lower than in Kirchhoff migration. The effect of noise on the amplitudes is studied in Figure 5. Both migration methods suffer to more or less the same extent from the noise. The amplitude errors rarely exceed the noise level of 30 % indicated by the box.

An analysis of a new migration method would not be complete without a test in the presence of a caustic. Therefore, we simulated a common-offset experiment over the trough structure depicted in Figure 6. The synthetic modeling was done by an implementation of the forward Kirchhoff-Helmholtz integral to include realistic diffraction events. The results of demodeling and Kirchhoff depth migration are compared in Figure 7. As we can see, demodeling provides as good a position of the

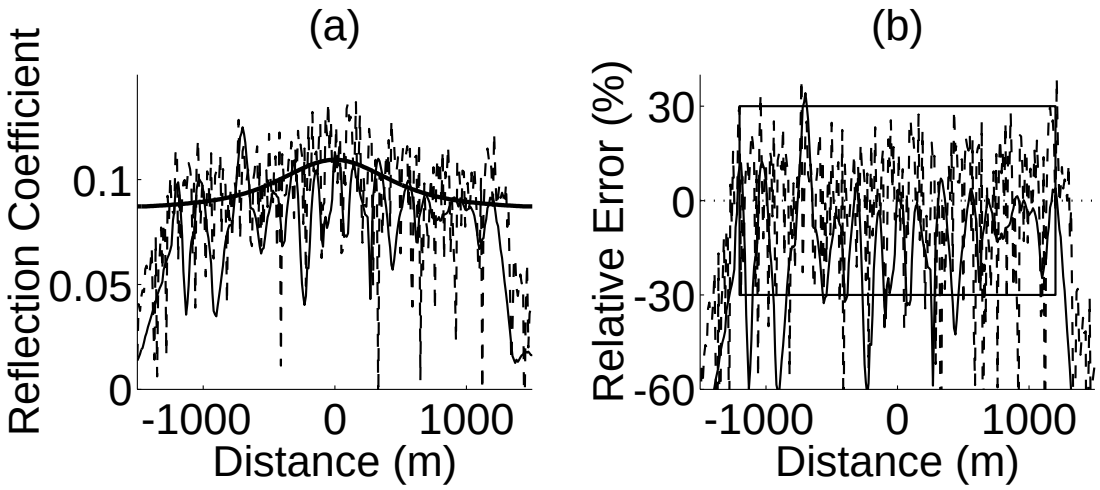

Figure 5: (a) Amplitudes along the reflector from demodeling (solid line) and Kirchhoff migration (dashed line) in comparison to reflection coefficients (bold line). (b) Relative errors.

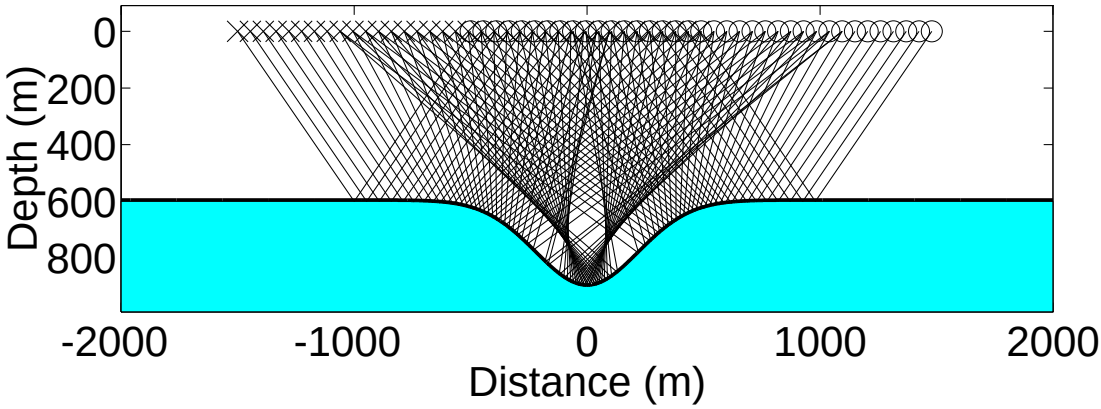

Figure 6: Model II: A trough structure below a homogeneous overburden.

migrated reflector image as Kirchhoff migration. The principal drawback of demodeling is noted when comparing the amplitudes along the reflector (Figure 8). Because of the presence of the diffractions, the amplitudes on flanks of the trough are not correctly recovered. In the range between -500 m and 500 m (except a small region around the origin), the error strongly fluctuates and exceeds 50%. Further investigations on how to distinguish reflections from diffractions and how to separate conflicting events in the picking process are envisaged to improve demodeling amplitudes in caustic regions.

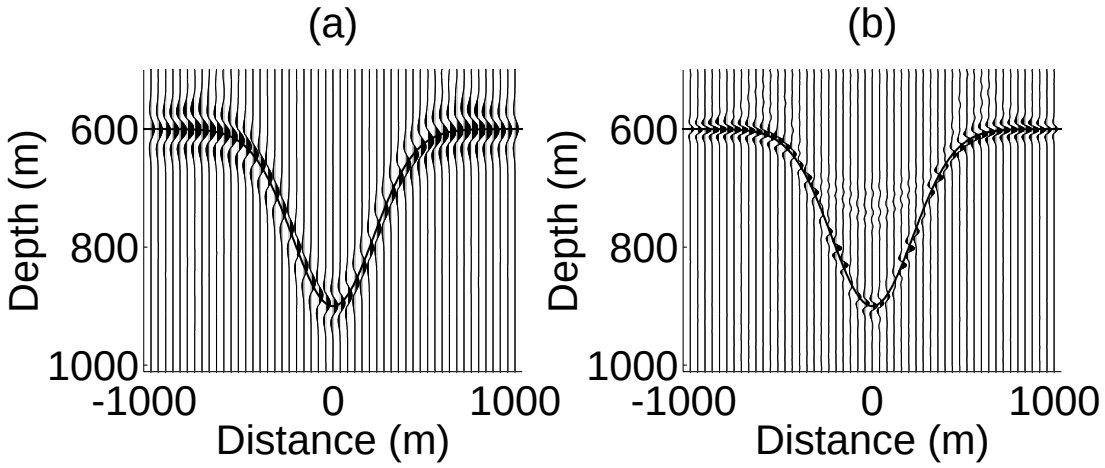

Figure 7: (a) Kirchhoff depth migrated section, (b) Kirchhoff demodeled section, of noise-free common-offset data for Model II.

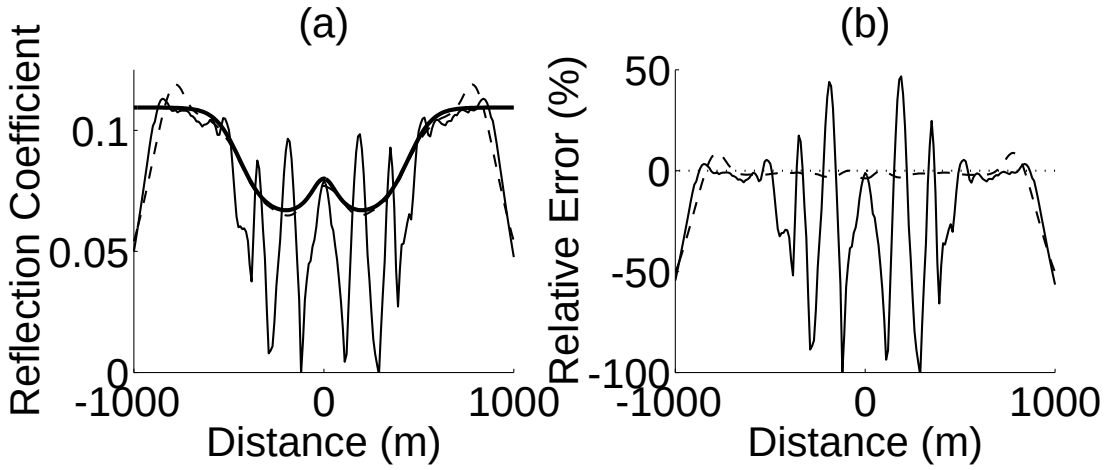

Figure 8: (a) Amplitudes along the reflector from demodeling (solid line) and Kirchhoff migration (dashed line) in comparison to reflection coefficients (bold line). (b) Relative errors.

CONCLUSIONS

We have presented a numerical analysis of a new migration method based on the Kirchhoff-Helmholtz integral. Since the process under investigation represents an (asymptotic) inverse to Kirchhoff modeling, we have termed it *Kirchhoff demodeling*. The demodeling integral is completely analogous to the modeling integral in the sense that it does exactly the same procedure along the reflection traveltime surface that the modeling integral does along the reflector.

By our numerical analysis, we have confirmed that demodeling can indeed be used for migration purposes. In all our experiments, demodeling correctly positioned the reflector in depth. Concerning amplitudes, demodeling presents positive as well as negative properties. Positively is to be noted that, under ideal circumstances, demodeling recovers the reflection coefficients along the reflecting interface with very small errors. Boundary zones can be kept smaller than in Kirchhoff migration. Random noise does not affect demodeling amplitudes any more than it does Kirchhoff migration. Off the reflector, the noise level is reduced by demodeling. As a negative quality of demodeling, its bad amplitude recovery in the presence of caustics is to be cited.

From an implementational point of view, we want to stress the following differences between Kirchhoff migration and demodeling. Because of the structure of the underlying integrals, demodeling is much faster than Kirchhoff migration, even when applied with full true-amplitude weights. We remind that the demodeling process is analogous to that of Kirchhoff modeling and, thus, needs comparable computing time. Like Kirchhoff migration, demodeling is a target-oriented migration method. However, contrary to Kirchhoff migration, where a *target zone* needs to be specified, demodeling can directly be restricted to a *target reflector.*

As a disadvantage, we remind that demodeling requires an identification and picking of the events to be migrated. In consequence, its result may vary with the picking algorithm used. For a kinematic migration, traveltime picking is sufficient. For true-amplitude migration, amplitude picking is also necessary. This should, however, not pose a severe restriction to the applicability of the method since the identification of horizons of interest is always necessary at some stage of the seismic processing sequence.

In conclusion, the new process is not to be seen as replacement of Kirchhoff migration, but as an alternative and complementary procedure. Possible applications include the fast true-amplitude migration of an identified event to determine whether a promising AVO trend in the CMP section is confirmed after migration.

ACKNOWLEDGEMENTS

The research of this paper was supported in part by the National Research Council (CNPq – Brazil), the Sao Paulo State Research Foundation (FAPESP – Brazil), and the sponsors of the WIT Consortium.

REFERENCES

Bojarski, N., 1982, A survey of the near-field far-field inverse scattering inverse source integral equation: IEEE Trans. Ant. Prop., **AP-30**, no. 5, 975–979.

Langenberg, K., 1986, Applied inverse problems for acoustic, electromagnetic, and elastic wave scattering *in* Sabatier, P., Ed., Basic methods in Tomography and Inverse Problems:: Adam Hilger.

Martins, J., Schleicher, J., Tygel, M., and Santos, L., 1997, 2.5-d true-amplitude Kirchhoff migration and demigration: J. Seism. Expl., **6**, no. 2/3, 159–180.

Porter, R., 1970, Diffraction-limited scalar image formation with holograms of arbitrary shape: J. Acoust. Soc. Am., **60**, no. 8, 1051–1059.

Ricker, N., 1953, The form and laws of propagation of seismic wavelets: Geophysics, **18**, no. 01, 10–40.

Rockwell, D., 1971, Migration stack aids interpretation: Oil and Gas Journal, **69**, 202–218.

Schneider, W., 1978, Integral formulation for migration in two and three dimensions: Geophysics, **43**, no. 1, 49–76.

Sommerfeld, A., 1964, Optics:, volume IV of **Lectures on Theoretical Physics** Academic Press, New York.

Tygel, M., Schleicher, J., and Hubral, P., 1995, Dualities between reflectors and reflection-time surfaces: J. Seis. Expl., **4**, no. 2, 123–150.

Tygel, M., Schleicher, J., Santos, L., and Hubral, P., 2000, An asymptotic inverse to the Kirchhoff-Helmholtz integral: Inv. Probl., **16**, 425–445.

PUBLICATIONS

The general derivation of the demodeling integral in inhomogeneous media was published in (Tygel et al., 2000).

APPENDIX A

2.5-D CONSTANT VELOCITY FORMULAS

In this appendix we investigate briefly the form of the Inverse Kirchhoff-Helmholtz integral (Tygel et al., 2000),

$$I(\vec{x},z) = -\frac{1}{4\pi}\int d\Gamma\ \mathcal{W}(\vec{x},\vec{\xi})\mathcal{A}(\vec{\xi})\ \partial_n F(z-\mathcal{Z}(\vec{x},\vec{\xi},t))|_{t=\Gamma(\vec{\xi})}\ . \qquad \text{(A-1)}$$

for the 2.5D case in constant-velocity media. In the above formula, $\vec{x} = (x, y)$, $\vec{\xi} = (\xi, \eta)$, $t = \Gamma(\vec{\xi})$ is the traveltime curve and $\mathcal{A}$ is the amplitude of the event with pulse shape $F(t)$ found in the seismic trace at Γ. Also, ∂_n denotes the partial derivative in the direction of the normal $\vec{n}$ to Γ and $\mathcal{Z}(\vec{x}, \vec{\xi}, t)$ is the isochron function defined implicitly by

$$\mathcal{T}(\vec{\xi}, \vec{x}, \mathcal{Z}) = t = \text{constant} \ , \tag{A-2}$$

where $\mathcal{T}(\vec{\xi}, \vec{x}, z)$ is the traveltime from the source-point $S(\vec{\xi})$ to the depth-point $(\vec{x}, z)$ and back to the receiver-point $G(\vec{\xi})$. To garantee correct amplitude recovery, the kernel $\mathcal{W}$ is selected as

$$\mathcal{W}(\vec{x}, \vec{\xi}) = \frac{h_B v^3 \cos^2\theta}{\cos^2\alpha} \mathcal{L}_S \mathcal{L}_G \ , \tag{A-3}$$

where v is the medium velocity at $M = (\vec{x}, \mathcal{Z}(\vec{x}, \vec{\xi}, \Gamma))$, and $\mathcal{L}_S$ and $\mathcal{L}_G$ are the the point-source geometrical-spreading factors along the ray segments SM ans MG, respectively. Moreover, θ represents the angle the normal to Γ makes with the vertical t-axis, and α denotes the incidence angle that the incoming ray SM makes with the isochron normal at M. Finally, h_B is the modulus of the Beylkin determinant,

$$h_B = \det \begin{vmatrix} \nabla_x \mathcal{T}(\vec{\xi}, M) \\ \partial_\xi \nabla_x \mathcal{T}(\vec{\xi}, M) \\ \partial_\eta \nabla_x \mathcal{T}(\vec{\xi}, M) \end{vmatrix} \ , \tag{A-4}$$

where $\nabla_x = (\partial_x, \partial_y, \partial_z)$ is the spatial gradient operator.

In the 2.5D case, and assuming, without loss of generality, that y and η are the simmetry axes, we may write $\vec{x} = (x, 0)$, $\mathcal{A}(\vec{\xi}) = \mathcal{A}(\xi)$, $\Gamma(\vec{\xi}) = \Gamma(\xi)$, $S(\vec{\xi}) = (x_S(\xi), 0)$ and $G(\vec{\xi}) = (x_G(\xi), 0)$. We also define the midpoint and half-offset coordinates,

$$m = \frac{x_S + x_G}{2} \ , \quad \text{and} \quad h = \frac{x_G - x_S}{2} \ . \tag{A-5}$$

In the above integral (A-1), the normal direction is not properly defined, since the t- and $\vec{\xi}$-coordinates have different dimensions. In order to overcome this problem, we must change the scale of the t-axis. For constant v, we define the new depth coordinate as $\zeta = vt$, so that it has the same dimension (length) as the $\vec{\xi}$-axes. In the new coordinates, the traveltime surface is given by $\zeta = v\Gamma(\vec{\xi})$. The integral (A-1) is therefore,

$$I(x, z) = \frac{1}{4\pi} \int d\xi d\eta \ \mathcal{W}(x, \vec{\xi}) \ \mathcal{A}(\xi) \ [\vec{n} \cdot \nabla_\xi \mathcal{Z}(x, \vec{\xi}, \zeta/v)]_{\zeta = v\Gamma} \ \partial_z F(z - \mathcal{Z}(x, \vec{\xi}, \Gamma)) \ , \tag{A-6}$$

where $\nabla_\xi = (\partial_\xi, \partial_\eta, \partial_\zeta)$. Note that now the non-unitary surface normal $\vec{n} = (v\Gamma', 0, -1)$ is well defined. Moreover, from now on, the prime will indicate derivative with respect to the horizontal-coordinate ξ.

To make use of the simmetry of the 2.5D situation, we transform integral (A-6) into the frequency domain, where it reads

$$I(x,k_z) = \frac{ik_z\mathcal{F}(k_z)}{4\pi}\int d\xi d\eta\, \mathcal{W}(x,\vec{\xi})\, \mathcal{A}(\xi)\, [\vec{n}\cdot\nabla_\xi \mathcal{Z}(x,\vec{\xi},\zeta/v)]_{\zeta=v\Gamma}\, \exp\{-ik_z\mathcal{Z}(x,\vec{\xi},\Gamma)\}\ . \tag{A-7}$$

Here, $\mathcal{F}$ denotes the Fourier transform of F.

The isochron $z = \mathcal{Z}(x,\vec{\xi},\zeta)$ corresponding to a constant time, can be easily evaluated as the half-ellipsoid of revolution with center at $(m,0,0)$ and semi-axes

$$a = \frac{vt}{2} = \frac{\zeta}{2}\ , \quad \text{and} \quad b = \sqrt{a^2-h^2}\ . \tag{A-8}$$

In symbols, we have the isochron

$$\mathcal{Z}(x,\vec{\xi},\zeta) = b\sqrt{1-\frac{(x-m)^2}{a^2}-\frac{\eta^2}{b^2}}\ . \tag{A-9}$$

The Beylkin determinant (A-4), in this case, reduces to (see Martins et al., 1997)

$$h_B = \frac{2\mathcal{Z}\cos^2\alpha}{v^3}\cdot\left(\frac{x'_S}{\mathcal{L}_S^2}+\frac{x'_G}{\mathcal{L}_G^2}\right)\cdot\left(\frac{1}{\mathcal{L}_S}+\frac{1}{\mathcal{L}_G}\right)\ , \tag{A-10}$$

with

$$\mathcal{L}_S = \sqrt{(x_S-x)^2+\mathcal{Z}^2}\ , \quad \text{and} \quad \mathcal{L}_G = \sqrt{(x_G-x)^2+\mathcal{Z}^2}\ . \tag{A-11}$$

Note that we do not need to compute $\cos^2\alpha$, since it will be canceled in the computation of the kernel (A-3). The last quantity we need is $\cos^2\theta$, which is given by

$$\cos^2\theta = 1+(v\Gamma'(\xi))^2\ . \tag{A-12}$$

Therefore, the expression for the kernel (A-3) is

$$\mathcal{W}(x,\xi,\eta) = 2\,[1+(v\Gamma'(\xi))^2]\,\mathcal{Z}\,[\mathcal{L}_S+\mathcal{L}_G]\,\left[\frac{x'_S}{\mathcal{L}_G^2}+\frac{x'_G}{\mathcal{L}_S^2}\right]\ . \tag{A-13}$$

We also must compute the gradiente $\nabla_\xi\mathcal{Z}$. After some algebraic manipulation, we find

$$\partial_\xi\mathcal{Z} = \frac{\gamma}{2\mathcal{Z}a^2}\ , \quad \partial_\eta\mathcal{Z} = -\frac{\eta}{\mathcal{Z}}\ , \quad \text{and} \quad \partial_\zeta\mathcal{Z} = \frac{a^4-h^2(x-m)^2}{2\mathcal{Z}a^3}\ , \tag{A-14}$$

where,

$$\gamma = b^2(x-m)(x'_S+x'_G)+h(x'_S-x'_G)(a^2-(x-m)^2)\ . \tag{A-15}$$

Now we are ready to approximate the integral in η by the stationary phase method. The general formula states that for $|k| \to \infty$,

$$\int d\eta\ \varphi(\eta)\ \exp\{-ik\psi(\eta)\} \approx \sqrt{\frac{2\pi}{i\ k\ \psi''(\eta^*)}}\ \varphi(\eta^*)\ \exp\{-ik\psi(\eta^*)\}\ , \qquad \text{(A-16)}$$

where η^* is the first-order stationary point of ψ, i.e., $\psi'(\eta^*) = 0$ and $\psi''(\eta^*) \neq 0$. In our case, $\psi(\eta) = \mathcal{Z}(x, \xi, \eta)$, $\eta^* = 0$, $\psi''(0) = \partial_\eta^2 \mathcal{Z} = -1/\mathcal{Z}$ and $\psi(0) = \mathcal{Z}$.

Applying all the results above to the integral in η in equation (A-7), we find

$$I(x, k_z) = \mathcal{F}(k_z) \sqrt{\frac{-ik_z}{2\pi}} \int d\xi\ \mathcal{A}(\xi)\ \mathcal{W}\ [\partial_\zeta \mathcal{Z} - v\Gamma' \partial_\xi \mathcal{Z}]\ \sqrt{\mathcal{Z}}\ \exp\{-ik_z \mathcal{Z}\}\ . \qquad \text{(A-17)}$$

Substituting the kernel $\mathcal{W}$ given by equation (A-13), we finally arrive at

$$\begin{aligned} I(x, k_z) \quad = \quad & \mathcal{F}(k_z) \sqrt{\frac{-ik_z}{2\pi}} \int d\xi\ \mathcal{A}(\xi)\ [\mathcal{L}_S + \mathcal{L}_G]\ \left[\frac{x'_S}{\mathcal{L}_G^2} + \frac{x'_G}{\mathcal{L}_S^2}\right]\ [1 + (v\Gamma')^2] \\ & (a^4 - h^2(x-m)^2 - av\Gamma'\gamma)\ \frac{\sqrt{\mathcal{Z}}}{2a^3}\ \exp\{-ik_z \mathcal{Z}\}\ , \end{aligned} \qquad \text{(A-18)}$$

or, equivalently in time-domain,

$$I(x, z) = \frac{1}{\sqrt{2\pi}}\ \int d\xi\ \mathcal{A}(\xi)\ \mathcal{W}_{2.5}(x, \xi)\ \mathcal{D}_z F(z - \mathcal{Z}(x, \xi, \Gamma))\ , \qquad \text{(A-19)}$$

where $\mathcal{D}_z$ denotes the depth-reverse half-derivative, which is equivalent to multiply by $\sqrt{-ik_z}$ in frequency domain, and where the 2.5D weight function for constant velocity is given by

$$\mathcal{W}_{2.5}(x, \xi) = [\mathcal{L}_S + \mathcal{L}_G]\ \left[\frac{x'_S}{\mathcal{L}_G^2} + \frac{x'_G}{\mathcal{L}_S^2}\right]\ [1 + (v\Gamma')^2]\ (a^4 - h^2(x-m)^2 - av\Gamma'\gamma)\ \frac{\sqrt{\mathcal{Z}}}{2a^3}\ . \qquad \text{(A-20)}$$